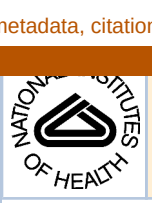

Published in final edited form as:

Magn Reson Med. 2010 February ; 63(2): 322–329. doi:10.1002/mrm.22225.

Hyperpolarized ^{13}C Spectroscopy and an NMR-Compatible Bioreactor System for the Investigation of Real-Time Cellular Metabolism

Kayvan R. Keshari[1,2], **John Kurhanewicz**[1], **Rex E. Jeffries**[2], **David M. Wilson**[1], **Brian J. Dewar**[2], **Mark Van Criekinge**[1], **Matthew Zierhut**[1], **Daniel B. Vigneron**[1], and **Jeffrey M. Macdonald**[2,*]

[1] Department of Radiology, University of California San Francisco, San Francisco, California, USA

[2] Department of Biomedical Engineering, University of North Carolina Chapel Hill, Chapel Hill, North Carolina, USA

Abstract

The purpose of this study was to combine a three-dimensional NMR-compatible bioreactor with hyperpolarized ^{13}C NMR spectroscopy in order to probe cellular metabolism in real time. JM1 (immortalized rat hepatoma) cells were cultured in a three-dimensional NMR-compatible fluidized bioreactor. ^{31}P spectra were acquired before and after each injection of hyperpolarized [1-^{13}C] pyruvate and subsequent ^{13}C spectroscopy at 11.7 T. ^{1}H and two-dimensional ^{1}H-^{1}H-total correlation spectroscopy spectra were acquired from extracts of cells grown in uniformly labeled ^{13}C-glucose, on a 16.4 T, to determine ^{13}C fractional enrichment and distribution of ^{13}C label. JM1 cells were found to have a high rate of aerobic glycolysis in both two-dimensional culture and in the bioreactor, with 85% of the ^{13}C label from uniformly labeled ^{13}C-glucose being present as either lactate or alanine after 23 h. Flux measurements of pyruvate through lactate dehydrogenase and alanine aminotransferase in the bioreactor system were 12.18 ± 0.49 nmols/sec/10^8 cells and 2.39 ± 0.30 nmols/sec/10^8 cells, respectively, were reproducible in the same bioreactor, and were not significantly different over the course of 2 days. Although this preliminary study involved immortalized cells, this combination of technologies can be extended to the real-time metabolic exploration of primary benign and cancerous cells and tissues prior to and after therapy.

Keywords

hyperpolarized; carbon; DNP; metabolism; flux; bioreactor

There is growing interest in the changes in fluxes through a variety of metabolic pathways associated with the evolution and progression of cancer (1–7) and its response to therapy. Recently, dynamic nuclear polarization (DNP) spectroscopic techniques have been used to study these metabolic fluxes in real time (8,9). Focus has been placed on changes in pathways associated with lipid synthesis and degradation (10,11), bioenergetics (12,13), and redox potential (14,15). Increases in lactate dehydrogenase (LDH) activity (8,9), changes in glutaminolysis (2), and decreases in pyruvate kinase activity (1) have been associated with cancer. These studies have been conducted primarily in extracts of cell cultures (3) or by way of in vivo animal studies (16–18). Cell culture studies provide a controlled platform for long-

*Correspondence to: Jeffrey M. Macdonald, Ph.D., Department of Biomedical Engineering, 152 MacNider Hall, Campus Box 7575, Chapel Hill, NC 27599-7575. jmacdona@med.unc.edu.

term metabolic studies, but they are tedious since each measurement requires new cells. In contrast, in in vivo studies the same animal can be used for multiple metabolic measurements, but they are more costly, are biologically heterogeneous, require many animals to be sacrificed, and are inefficient for the initial screening of novel metabolic tracers.

For the last 3 decades, cell perfusion or "bioreactor" systems have been developed in an attempt to address these fundamental issues (15,19,20). These three-dimensional culture perfusion systems have allowed the monitoring of steady-state metabolites and their changes with time (21,22), typically through the analysis of output parameters such as concentrations of lactate, glucose, and alanine in media (23). Studies have also been performed in order to assess slow metabolic processes, such as phospholipid (24), glutathione (25), and glutamine metabolism (26), but these systems do not have the temporal resolution to study fast kinetic reactions.

Due to the dynamic nature of cellular metabolism and its instantaneous response to changing stimuli (environmental, genetic, etc.) the study of flux through pathways, now dubbed "fluxomics", has become a rapidly expanding area of research in metabolomics (27,28). An inherent problem associated with determining real-time fluxes is the speed of some metabolic reactions. Enzymes of clinical interest, such as LDH, have been measured to have relatively high velocities (29), and thus measurement of flux through LDH in a living system is difficult. While glucose conversion to lactate by ^{13}C NMR has been achieved, it has involved long glucose infusion periods relative to the rates of the reactions in tissues of interest (30). A great deal of work has been done determining steady-state metabolite concentrations and inferring metabolic flux by mass spectrometry (31), NMR (32), and spectrophotometry (33). However, these traditional methods require the system to be quenched and extracted for each time point necessary to calculate flux. NMR spectroscopy is a research tool that can be readily translated to the clinic. ^{13}C NMR spectroscopy provides high spectral resolution and has been used to study metabolic fluxes in a variety of systems (34). The major shortcoming of ^{13}C NMR spectroscopy is its lack of sensitivity due to a low gyromagnetic ratio (γ), resulting in the inability to measure flux with high spatial and temporal resolution. This major hindrance has been recently overcome through the development of DNP NMR spectroscopy (35). ^{13}C-labeled substrates have been recently polarized using DNP techniques to obtain tens-of-thousands-fold enhancement of ^{13}C NMR signals of the substrate and its metabolic products, enabling measurement of rapid metabolic fluxes such as those catalyzed by LDH and alanine aminotransaminase (ALT).

Recent studies of hyperpolarized ^{13}C-labeled compounds, by way of the DNP method (8,9, 36), have been used to investigate metabolic processes associated with increases in aerobic glycolysis, deemed the Warburg effect (36,37). The Warburg intermediates (elevated lactate, alanine, and pyruvate) have been used as a way to characterize cancer aggressiveness (8) and response to therapy (9). In this study, JM1 (immortalized rat hepatoma) cells were cultured in a three-dimensional NMR-compatible bioreactor (38), and injections of hyperpolarized [1-^{13}C] pyruvate were used to serially measure LDH and ALT fluxes in real time.

MATERIALS AND METHODS

Cell Culture and Bioreactor

JM1 rat hepatoma cells (Michalopoulos Lab, University of Pittsburgh, PA) were cultured in Dulbecco's modified Eagle's medium (Invitrogen; 3 g/L glucose) supplemented with 10% fetal calf serum, 100 units/mL penicillin, and 100 μg/mL streptomycin (Invitrogen, Carlsbad, CA). Cells were grown in T150-flasks (Fisher Scientific, Pittsburgh, PA) to incubated at 37°C in a 95% air/5% CO_2 incubator. For two-dimensional (2D) culture extract experiments, cells were plated on 150-cm^2 coated plates (Fisher Scientific) and grown to less than 90% confluency (12.6×10^6 cells). Medium was changed for each plate and replaced with analogous medium

supplemented with uniformly labeled ^{13}C-glucose (Cambridge Isotope Labs, Andover, MA). Plates were allowed to progress for 23 h (n = 4). At each time point, an aliquot of medium was collected, and plates were washed twice with ice-cold phosphate-buffered saline and extracted in ice-cold methanol as previously described (39). Residual pellets were also extracted in deuterated chloroform to assess the labeling of lipids (40). Fractional enrichment (FE) was defined as the percentage of ^{13}C-labeled compound relative to the total pool.

For bioreactor experiments, cells were trypsinized, washed in phosphate-buffered saline, and electrostatically encapsulated at a concentrations of 25 (n = 1), 50 (n = 2), and 127 × 10^6 (n = 1) cells/mL in 500-μm beads, as previously described (41). Approximately 1.5 mL of encapsulates was perfused using the same medium formulation as above, recirculated at a rate of 4 mL/min. The bioreactor loop contains 40 mL in circulation. Medium was kept at a constant 37°C by way of water-jacketed lines, and gas pressures were maintained by a gas exchange module using 95% air/5% CO_2 gas, as previously described (42). A schematic of the bioreactor system is shown in Fig. 1. Encapsulates were removed at the end of the experiment, embedded in optimal cutting temperature, and stained with hematoxylin and eosin as previously described (7) to confirm cells were greater than 90% viable.

Hyperpolarization Methods

[1-^{13}C]-pyruvate was hyperpolarized by the DNP method (35) using the Hypersense® (Oxford Instruments, Oxford, UK) to an average polarization of ~15%. The compound polarized was a mixture of [1-^{13}C]-pyruvic acid (14.2 M) and the trityl radical (15 mM; tris[8-carboxyl-2,2,6,6-tetra[2-(1-hydroxyethyl)]-benzo(1,2-d:4,5-d)bis(1,3)dithiole-4-yl]methyl sodium salt) (GE Health, Menlo Park, CA). Samples were dissolved in a dissolution solution containing $NaPO_4$ (50 mM)/ethylenediaminetetraacetic acid (EDTA) (0.3 mM) to bring the sample to the desired concentration and average pH of 7.5. A solution of 1 mL of the hyperpolarized pyruvate was injected into the bioreactor system with continuous flow, resulting in a final concentration of between 2- and 14-mM pyruvate. Higher concentrations were used in bioreactors, which contained a higher cell concentration. This was done to keep the same relative substrate concentration throughout the group of bioreactors. The bioreactor is water jacked and there were no observed temperature changes in the cell mass during the studies. These concentrations were kept constant relative to the encapsulated cell concentration, allowing the cell suspension to see an analogous influx of mass of pyruvate at each injection.

NMR Acquisition and Analysis

Cell extract samples were placed in a Speed-Vac® for 8 h to evaporate the methanol. Cell pellets were then reconstituted in 100% deuterium oxide (D_2O) (with 2.5 mM 3-(trimethylsilyl) propionic acid (TSP) both from Sigma-Aldrich, St. Louis, MO for quantification). Media aliquots were supplemented with 10% D_2O (and a final concentration of 2.5 mM TSP). ^{1}H and 2D ^{1}H-^{1}H total correlation spectroscopy spectra were acquired at 16.4 T on a Varian INOVA (700-MHz ^{1}H; Varian Instruments, Palo Alto, CA) equipped with 5mm ^{1}H/^{13}C indirect probe at 25°C. ^{1}H spectra of extracts were acquired using a total pulse repetition time of 12.65 sec, number of transients of 64, and a 90° flip angle. Data were analyzed using ACD Labs 9.0 1D NMR Processor (ACD Labs, Toronto, Ontario). ^{1}H spectra were zero filled to 32,000 points, line broadened 0.5 Hz using an exponential gaussian function. Peaks and ^{13}C satellites corresponding to glucose, lactate, alanine, glutamate, and the nucleotide spin systems of the purines and pyrimidines (AXP+GXP, UXP+CXP) were peak fit and quantified relative to TSP in ACD, as previously described (34,43).

2D total correlation spectroscopy (TOCSY) data were acquired with pulse repetition time = 2.48 sec, number of transients = 16, and number of indirect dimension increments of 64. Data were linear predicted in 3 × N in the indirect dimension and zero filled to 2000 points. The data

were 2D Fourier transformed, and cross-peaks corresponding to unlabeled and ^{13}C-labeled lactate, alanine, glutamate, and the ribose of nucleotides were volume integrated, as previously described (34). These points were then used to calculate FE as the sum of the of center cross-peaks to the total volume. The peak areas from the one-dimensional ^{1}H and volumes from the 2D ^{1}H-^{1}H total correlation spectroscopy (TOCSY) were used to calculate the absolute number of millimoles of each compound that was generated as a result of uniformly labeled ^{13}C-glucose metabolism.

For bioreactor studies, ^{13}C and ^{31}P spectra were acquired on an 11.7-T Varian INOVA (125-MHz ^{13}C and 202-MHz ^{31}P; Varian Instruments) equipped with a 10mm, triple-tune, direct-detect, broadband probe at 37°C. ^{31}P time courses were acquired before and after hyperpolarized injections, using a pulse repetition time = 3 sec, number of transients = 1024, and a 90° flip angle. ^{31}P spectra were zero filled to 40,000 points and line broadened 15 Hz. Assessment of changes in the β-nucleotide triphosphate (βNTP) resonances as a function of time was used to monitor cell health through the progression of the bioreactor experiments in vivo. Hyperpolarized ^{13}C experiments were acquired using a 5° flip angle and pulse repetition time = 3 sec and acquired for 300 sec. Data were zero filled to 16,000 points and line broadened 5 Hz. The resonances of pyruvate (171 ppm), lactate (182 ppm) and alanine (175 ppm) were integrated and compared as a function of time to determine the characteristics of enzymatic interconversion as a result of pyruvate injections. Fluxes were determined using a model of LDH and ALT labeling flux implemented in Interactive Data Language (ITT Visual Information Solutions, Boulder, CO) normalized for injected hyperpolarized pyruvate concentration and cell concentration estimated from relative changes in βNTP peak area. Briefly, the pyruvate peak area over time (M_p) was modeled to determine the arrival time (t_a), rate of injection (k_i), and signal decay of pyruvate (k_p).

$$M_p(t)=\begin{cases} \frac{k_i}{k_p}(1-e^{-k_p(t-t_a)}) & \forall t_a \le t<t_e \\ M_p(t_e)e^{-k_p(t-t_e)} & \forall t \ge t_e \end{cases} \quad [1]$$

The t_e represents the end of the pyruvate injection time. These fitted parameters were then used to fit the ^{13}C lactate and alanine data to estimate LDH and ALT labeling fluxes (k_{px}), where x represents either lactate or alanine (2).

$$M_p(t)=\begin{cases} \frac{k_{px}k_i}{k_p-k_x}\left(\frac{1-e^{-k_x(t-t_a)}}{k_x}-\frac{1-e^{-k_p(t-t_a)}}{k_p}\right) & \forall t_a \le t<t_e \\ \frac{M_p(t_e)k_{px}}{k_p-k_x}(e^{-k_x(t-t_e)}-e^{-k_p(t-t_e)}) & \\ \quad +M_x(t_e)e^{-k_x(t-t_e)} & \forall t \ge t_e \end{cases} \quad [2]$$

One pool of pyruvate, lactate, and alanine was assumed in this model. In contrast to the model described by Day and coworkers (9), this model includes the rate of injection, which is a result of the flow of material into the bioreactor. This is not necessary in a model of cells in a nonperfused system but is important when small tip angles are used to assess magnetization as the substrate is flowing into the system. The exchange of lactate and alanine back to pyruvate was not included in this model, and therefore we are not measuring a kinetic constant but purely a measure of hyperpolarized label generation in time, or overall flux, which is specific for a given cell line or tissue under a given set of conditions. The large amount of hyperpolarized lactate observed in this study is consistent with the high LDH K_{eq} in favor of lactate (44), as well as in prior in vivo studies of hyperpolarized [1-^{13}C] pyruvate (8,9,36,45).

RESULTS AND DISCUSSION

Extracts of 2D Cultures and Determination of the Mass Balance of Uniformly Labeled ^{13}C-Glucose

Figure 2a is a representative ^{1}H spectrum of the aliphatic region obtained from a methanol extraction of JM1 cells after metabolism of ^{13}C-substrate for 23 h. ^{13}C satellites of lactate, alanine, glutamate (both as glutamate (Glut) and as the glutamyl group of the tripeptide glutathione (GSH)), and the nucleotide riboses (not pictured) are visible. The concentrations of these five compounds plus pyruvate and glucose in the initial medium formulation and at 23 h from the cell methanol extract and 2D culture media are given in Table 1. In comparison to normal rat liver (46), the JM1 rat hepatoma cell line produces significantly more lactate and alanine, and ribose (Table 1), demonstrating the Warburg effect and pentose phosphate pathway products for nucleotide synthesis, respectively. They also demonstrate a high concentration of glutathione, which has been observed in other cell lines such as MCF-7 human breast cancer (47) and DU145 prostate cancer cells (48). In fact, one of the largest resonances in the ^{1}H spectrum is from glutathione (Fig. 2a).

Representative regions of a typical 2D ^{1}H-^{1}H total correlation spectroscopy spectrum are shown in Fig. 2b, demonstrating cross-peaks used to determine the ^{13}C FE of the previously mentioned compounds. At 23 h, lactate and alanine FEs are 88.9 ± 2.9% and 57.8 ± 3.1%, respectively. The glutamate and glutamyl of GSH have FEs of 7.1 ± 2.2% and 10.1 ± 2.4%, respectively. The FEs of the ribose in nucleotides were similar for both purines and pyrimidines, enriching to 91.6 ± 2.7 and 91.5 ± 3.8%. It is important to note that after 5 min, the lactate pool inside the cell had an FE of 55.1 ± 7.9%, while that of alanine was 14.0 ± 5.9%. Glutamate labeling was not detectable at 5 min. Not surprising was that lipids were not labeled to a detectable level, likely because lipids form from anaplerotic products of the Krebs cycle. These intermediates were at most labeled to 10%, as can be inferred from the glutamate FE, and in turn could have internal labeled the lipids to a level below detection in this study.

By quantifying the absolute number of micromoles of ^{13}C for each compound at 23 h in the cell, a distribution of label can be generated, which is shown in Fig. 2c. Nearly 85% of the label is present as either lactate or alanine in JM1 cells after 23 h. Activity of the pentose phosphate pathway in converting glucose to the ribose backbone of nucleotides accounts for approximately 4.7% of the ^{13}C label distribution, while another 9.2% are resident in glutamate (half of which is GSH). At the 23 h time point, each 150-cm^2 plate of JM1 cells had produced 242.57 ± 15.79 μmol of lactate and 17.7 ± 1.53 μmol of alanine and exported it to the medium.

Bioreactor Cultures of JM1 Cells and ^{31}P NMR Studies

^{31}P spectra were used to monitor changes in cell energetics with growth over time. Figure 3a shows a representative 500-μm bead of encapsulated JM1 cells, cryo-sectioned and stained by hematoxylin and eosin at 20× magnification. JM1 cells were evenly distributed throughout the alginate beads and were predominantly spherical. Figure 3b shows a representative ^{31}P spectrum of JM1 cells encapsulated to a concentration of 1.2×10^8 cells/mL at 4 h of perfusion in the bioreactor. NMR signals for the phosphates of the NTPs (γNTP, αNTP, and βNTP), phosphocholine, inorganic phosphate, glycerol phosphocholine, glycerophosphoethanolamine, nicotinamide (reduced and oxidized), diphosphodiesters (most commonly (UDP) uridine diphosphate UDP-glucose) (15,16) and the sugar phosphate groups (sugar PO_4^{-3}) are readily visible.

Figure 4a shows a representative ^{31}P time course of βNTP changes of JM1 cells growing in the bioreactor over the time course of the bioreactor studies. The dotted red lines indicate the time of injection of hyperpolarized [1-^{13}C] pyruvate. Increases in βNTP correlate to the cell

concentration and are indicative of the cell growth with time (13,15,21,49). About 80% of βNTP is adenine nucleotide and about 90% is NMR visible in rat liver (50). As cells grew inside of the bioreactor, hyperpolarized [1-^{13}C] pyruvate was injected to assess conversion of pyruvate to its metabolic products. Figure 4b demonstrates ^{31}P spectra before and immediately after two injections of hyperpolarized [1-^{13}C] pyruvate at 4 and 18.5 h. Increases in the ^{31}P resonances at the later time point demonstrate that the cells not only survive the injection but also continue to grow over time.

Previous ^{31}P NMR studies of NMR-compatible bioreactors containing alginate-encapsulated transformed cells (51) showed that cells are viable for several days. Here we demonstrate that the cells double in a comparable period of time as in 2D cultures of JM1 (49). This is likely due to the uniform diameter of 500 μm, which was permitted by use of electrostatic encapsulation. In normal aerobic cells such as hepatocytes, the diffusion distance for oxygen is typically 200 μm; cells become hypoxic at greater diffusion distances (38,52). Transformed cells consume less oxygen than primary hepatocytes at 250 μm, the maximal diffusion distance in the 500-μm diameter encapsulates. Although an oxygen gradient is created in the 500-μm-diameter encapsulates, dictated by the diffusion coefficient and oxygen consumption rate, there would be little or no hypoxic zone within the encapsulate compared to previous studies that used >1mm diameter (51). In short, the relatively small and uniform diameter of the encapsulates permitted sufficient diffusion of hyperpolarized [1-^{13}C] pyruvate to the cells.

Bioreactor Cultures of JM1 Cells and ^{13}C NMR DNP Studies

Figure 4c demonstrates injections of 1 mL of 7.1-mM hyperpolarized [1-^{13}C] pyruvate at 4 h and 18.5 h in the same bioreactor system. Each ^{13}C spectrum is at 90 sec postinjection and shows the high signal-to-noise ratio of labeled lactate and alanine as a result of interconversion from the injected pyruvate. The spectrum on the right exhibits higher SNR, due to the characteristic cell growth over time of the JM1 cells in the bioreactor. Lactate and alanine production as a result of flux through LDH and ALT, respectively, was seen to scale with cell concentration, as expected.

Hyperpolarized ^{13}C spectra were integrated and time courses of lactate and alanine were generated. Figure 5 shows the ^{13}C spectrum of a bioreactor at 84 sec postinjection (Fig. 5a) and its representative signal over time (Fig. 5b). The influx of pyruvate as a result of the injection is shown, and peaks corresponding to its metabolic products, lactate and alanine, are observed within 2 scans (i.e., 6 sec) of the pyruvate signal. A representative time course of ^{13}C lactate, alanine, and pyruvate is shown in Fig. 5c. This data were fit to a two-state model of the interconversion of pyruvate to lactate and alanine, and the fit is shown as the solid line through the raw data. The flux rates of [1-^{13}C] pyruvate to [1-^{13}C] lactate and [1-^{13}C] alanine, facilitated by LDH and ALT, were determined to be 12.18 ± 0.49 nmols/sec/10^8 cells and 2.39 ± 0.30 nmols/sec/10^8 cells, respectively. The low standard error (SE) in the bioreactor supports the reproducibility of the system as a real-time measurement of the flux through LDH. The measurement for ALT flux exhibited a higher standard error, most likely due to the lower signal to noise of [1-^{13}C] alanine in hyperpolarized studies, in comparison to lactate. Figure 5d demonstrates the differences between flux measurements that were made on the first and second day in the bioreactor system. LDH flux and ALT flux were not found to be significantly different between the two days (P = 0.4 and 0.6, respectively). Multiple injections of hyperpolarized [1-^{13}C] pyruvate were done on all bioreactors, yielding similar results, thus reinforcing the robustness of not only the bioreactor system but also the flux measurement by hyperpolarized [1-^{13}C] pyruvate injection. These data suggest that differences in metabolic fluxes with cellular perturbations (i.e., changing oxygen tension, metabolic substrates, and/or therapy) as small as 5% can be measured in the bioreactor. Also, having accurate control over the bead size (500 μm) of the encapsulated cells provided an environment in which all cells

are equally perfused (i.e., the 250-μm diffusion limit was maintained), a situation that is closer to physiologic than provided by other NMR-compatible bioreactors (19,38,49,51).

The pyruvate metabolism in the bioreactor system, assessed by the DNP method, demonstrated fluxes through LDH and ALT analogous to those of glucose in the standard 2D culture system. Unlike the first cell study showing flux through LDH by DNP (9), concentrations in this study (Table 1) were closer to the physiologic conditions, as a result of continuous perfusion. The bolus of pyruvate creates a spike in pyruvate concentration that is similar for both perfused bioreactor and *in vivo* magnetic resonance spectroscopic imaging (MRSI) studies (1). Typically, the serum concentrations for these compounds are in the half to several millimolar range, and medium is near this range, except for glucose, which is several fold higher (25 mM [4.5g/L] vs 3.9 to 6.1 mM [0.7–1.1 g/L]) (52), as well as pyruvate, which is very low in serum (500 μM vs 100 μM). The goal of this study was to generate a model similar to an animal model. Although in both bioreactor and in vivo DNP studies a nonphysiologic bolus of pyruvate is given, a similar dose can be given in both cases for comparison of the ex vivo and in vivo fluxes. This information can be used in order to rapidly test novel molecules and save time, money, and animal lives for development of DNP imaging.

Metabolic fluxes, even for kinetically fast enzymes such as LDH, can be measured while maintaining cells in a physiologically viable state. This also allows for the monitoring of enzyme concentration, as well as real-time metabolism by way of modulation of substrate concentration. Combining ^{13}C labeling interleaved between hyperpolarized ^{13}C studies would allow for the assessment of both kinetically fast and slow metabolic processes. It must be noted that hyperpolarized ^{13}C studies may not be appropriate for measuring slower metabolic fluxes or sequential steps in an enzymatic pathway (i.e., flux to glutamate or fatty acids). However, the dramatic increase in sensitivity provided by DNP will potentially allow for the measurement of fast metabolic fluxes in people.

Summary

This study demonstrates that hyperpolarized ^{13}C NMR can be combined with an NMR-compatible bioreactor to measure metabolic fluxes in three-dimensional cell cultures. JM1 hepatoma cells were found to have a high rate of aerobic glycolysis in both conventional 2D culture and in the bioreactor. The high sensitivity of hyperpolarized ^{13}C NMR allowed the measurement of metabolic fluxes in real time. Although this preliminary study involved immortalized cells, this combination of technologies could be extended to the real-time metabolic exploration of primary benign and cancerous cells and tissues.

Acknowledgments

National Institutes of Health; Grant numbers: R21 EB007588, R21 GM075941.

The project was funded by the National Institutes of Health, NIH R21 EB007588 (J.K.) and R21 GM075941 (J.M.M.). We appreciate the technical support of Dr. Pediatidakis for acquisition and culture of JM1 cells.

References

1. Christofk H, Vander Heiden M, Harris M, Ramanathan A, Gerszten R, Wei R, Fleming M, Schreiber S, Cantley L. The M2 splice isoform of pyruvate kinase is important for cancer metabolism and tumour growth. Nature 2008;452:230–233. [PubMed: 18337823]
2. DeBerardinis RJ, Lum JJ, Hatzivassiliou G, Thompson CB. The biology of cancer: metabolic reprogramming fuels cell growth and proliferation. Cell Metab 2008;7:11–20. [PubMed: 18177721]
3. Fan TW, Kucia M, Jankowski K, Higashi RM, Ratajczak J, Ratajczak MZ, Lane AN. Rhabdomyosarcoma cells show an energy producing anabolic metabolic phenotype compared with primary myocytes. Mol Cancer 2008;7:79. [PubMed: 18939998]

4. Gatenby RA, Gillies RJ. Glycolysis in cancer: a potential target for therapy. Int J Biochem Cell Biol. 2007
5. Hsu PP, Sabatini DM. Cancer cell metabolism: Warburg and beyond. Cell 2008;134:703–707. [PubMed: 18775299]
6. Munger J, Bennett B, Parikh A, Feng X, Mcardle J, Rabitz H, Shenk T, Rabinowitz J. Systems-level metabolic flux profiling identifies fatty acid synthesis as a target for antiviral therapy. Nat Biotechnol 2008;26:1179–1186. [PubMed: 18820684]
7. Tessem M, Swanson MG, Keshari KR, Albers MJ, Joun D, Tabatabai ZL, Simko J, Shinohara K, Nelson SJ, Vigneron DB, Gribbestad IS, Kurhanewicz J. Evaluation of lactate and alanine as metabolic biomarkers of prostate cancer using ^{1}H HR-MAS spectroscopy of biopsy tissues. Magn Reson Med 2008;60:510–516. [PubMed: 18727052]
8. Albers MJ, Bok R, Chen AP, Cunningham CH, Zierhut ML, Zhang VY, Kohler SJ, Tropp J, Hurd RE, Yen YF, Nelson SJ, Vigneron DB, Kurhanewicz J. Hyperpolarized ^{13}C lactate, pyruvate, and alanine: noninvasive biomarkers for prostate cancer detection and grading. Cancer Res 2008;68:8607–8615. [PubMed: 18922937]
9. Day SE, Kettunen MI, Gallagher FA, Hu DE, Lerche M, Wolber J, Golman K, Ardenkjaer-Larsen JH, Brindle KM. Detecting tumor response to treatment using hyperpolarized ^{13}C magnetic resonance imaging and spectroscopy. Nat Med 2007;13:1382–1387. [PubMed: 17965722]
10. Ackerstaff E, Glunde K, Bhujwalla ZM. Choline phospholipid metabolism: a target in cancer cells? J Cell Biochem 2003;90:525–533. [PubMed: 14523987]
11. Iorio E, Mezzanzanica D, Alberti P, Spadaro F, Ramoni C, D'Ascenzo S, Millimaggi D, Pavan A, Dolo V, Canevari S, Podo F. Alterations of choline phospholipid metabolism in ovarian tumor progression. Cancer Res 2005;65:9369–9376. [PubMed: 16230400]
12. Bonarius HP, Ozemre A, Timmerarends B, Skrabal P, Tramper J, Schmid G, Heinzle E. Metabolic-flux analysis of continuously cultured hybridoma cells using (13)CO(2) mass spectrometry in combination with (13)C-lactate nuclear magnetic resonance spectroscopy and metabolite balancing. Biotechnol Bioeng 2001;74:528–538. [PubMed: 11494221]
13. Kurhanewicz J, Dahiya R, Macdonald JM, Jajodia P, Chang LH, James TL, Narayan P. Phosphorus metabolite characterization of human prostatic adenocarcinoma in a nude mouse model by ^{31}P magnetic resonance spectroscopy and high pressure liquid chromatography. NMR Biomed 1992;5:185–192. [PubMed: 1449954]
14. Thelwall PE, Yemin AY, Gillian TL, Simpson NE, Kasibhatla MS, Rabbani ZN, Macdonald JM, Blackband SJ, Gamcsik MP. Noninvasive in vivo detection of glutathione metabolism in tumors. Cancer Res 2005;65:10149–10153. [PubMed: 16287997]
15. Gillies RJ, Liu Z, Bhujwalla ZM. ^{31}P-MRS measurements of extracellular pH of tumors using 3-aminopropylphosphonate. Am J Physiol 1994;267(1 pt 1):C195–203. [PubMed: 8048479]
16. Macdonald JM, Schmidlin O, James TL. In vivo monitoring of hepatic glutathione in anesthetized rats by ^{13}C NMR. Magn Reson Med 2002;48:430–439. [PubMed: 12210907]
17. Jucker BM, Lee JY, Shulman RG. In vivo ^{13}C NMR measurements of hepatocellular tricarboxylic acid cycle flux. J Biol Chem 1998;273:12187–12194. [PubMed: 9575166]
18. van Zijl PC, Jones CK, Ren J, Malloy CR, Sherry AD. MRI detection of glycogen in vivo by using chemical exchange saturation transfer imaging (glycoCEST). Proc Natl Acad Sci USA 2007;104:4359–4364. [PubMed: 17360529]
19. Mancuso A, Fernandez EJ, Blanch HW, Clark DS. A nuclear magnetic resonance technique for determining hybridoma cell concentration in hollow fiber bioreactors. Biotechnology (NY) 1990;8:1282–1285.
20. Wolfe SP, Hsu E, Reid LM, Macdonald JM. A novel multi-coaxial hollow fiber bioreactor for adherent cell types, part 1: hydrodynamic studies. Biotechnol Bioeng 2002;77:83–90. [PubMed: 11745176]
21. Mancuso A, Zhu A, Beardsley NJ, Glickson JD, Wehrli S, Pickup S. Artificial tumor model suitable for monitoring ^{31}P and ^{13}C NMR spectroscopic changes during chemotherapy-induced apoptosis in human glioma cells. Magn Reson Med 2005;54:67–78. [PubMed: 15968647]
22. Farghali H, Caraceni P, Rilo HL, Borle AB, Gasbarrini A, Gavaler JS, Van Thiel DH. Biochemical and ^{31}P-NMR spectroscopic evaluation of immobilized perfused rat Sertoli cells. J Lab Clin Med 1996;128:408–416. [PubMed: 8833890]

23. Bailey, JE.; Ollis, DF. Biochemical engineering fundamentals. New York: McGraw-Hill; 1986. p. 928
24. Beloueche-Babari M, Jackson LE, Al-Saffar NM, Eccles SA, Raynaud FI, Workman P, Leach MO, Ronen SM. Identification of magnetic resonance detectable metabolic changes associated with inhibition of phosphoinositide 3-kinase signaling in human breast cancer cells. Mol Cancer Ther 2006;5:187–196. [PubMed: 16432178]
25. Gamcsik MP, Millis KK, Colvin OM. Noninvasive detection of elevated glutathione levels in MCF-7 cells resistant to 4-hydroperoxycyclophosphamide. Cancer Res 1995;55:2012–2016. [PubMed: 7743493]
26. DeBerardinis RJ, Mancuso A, Daikhin E, Nissim I, Yudkoff M, Wehrli S, Thompson CB. Beyond aerobic glycolysis: transformed cells can engage in glutamine metabolism that exceeds the requirement for protein and nucleotide synthesis. Proc Natl Acad Sci USA 2007;104:19345–19350. [PubMed: 18032601]
27. Droste P, Weitzel M, Wiechert W. Visual exploration of isotope labeling networks in 3D. Bioprocess Biosyst Eng 2008;31:227–239. [PubMed: 18074156]
28. Massou S, Nicolas C, Letisse F, Portais JC. NMR-based fluxomics: quantitative 2D NMR methods for isotopomers analysis. Phytochemistry 2007;68:2330–2340. [PubMed: 17466349]
29. Chowdhury SK, Gemin A, Singh G. High activity of mitochondrial glycerophosphate dehydrogenase and glycerophosphate-dependent ROS production in prostate cancer cell lines. Biochem Biophys Res Commun 2005;333:1139–1145. [PubMed: 15967408]
30. van der Zijden JP, van Eijsden P, de Graaf RA, Dijkhuizen RM. $^{1}H/^{13}C$ MR spectroscopic imaging of regionally specific metabolic alterations after experimental stroke. Brain 2008;131(pt 8):2209–2219. [PubMed: 18669496]
31. Miccheli A, Tomassini A, Puccetti C, Valerio M, Peluso G, Tuccillo F, Calvani M, Manetti C, Conti F. Metabolic profiling by ^{13}C-NMR spectroscopy: [1,2-$^{13}C2$]glucose reveals a heterogeneous metabolism in human leukemia T cells. Biochimie 2006;88:437–448. [PubMed: 16359766]
32. Burgess SC, Weis B, Jones JG, Smith E, Merritt ME, Margolis D, Dean Sherry A, Malloy CR. Noninvasive evaluation of liver metabolism by ^{2}H and ^{13}C NMR isotopomer analysis of human urine. Anal Biochem 2003;312:228–234. [PubMed: 12531210]
33. Stephanopoulos, G.; Gill, RT. Metabolic engineering. Nielsen, J., editor. Heidelberg: Springer Berlin; 2001.
34. Lane AN, Fan TWM. Quantification and identification of isotopomer distributions of metabolites in crude cell extracts using ^{1}H TOCSY. Metabolomics 2007;3:79–86.
35. Ardenkjaer-Larsen JH, Fridlund B, Gram A, Hansson G, Hansson L, Lerche MH, Servin R, Thaning M, Golman K. Increase in signal-to-noise ratio of > 10,000 times in liquid-state NMR. Proc Natl Acad Sci USA 2003;100:10158–10163. [PubMed: 12930897]
36. Chen AP, Albers MJ, Cunningham CH, Kohler SJ, Yen YF, Hurd RE, Tropp J, Bok R, Pauly JM, Nelson SJ, Kurhanewicz J, Vigneron DB. Hyperpolarized C-13 spectroscopic imaging of the TRAMP mouse at 3T-initial experience. Magn Reson Med 2007;58:1099–1106. [PubMed: 17969006]
37. Warburg O. On the origin of cancer cells. Science 1956;123:309–314. [PubMed: 13298683]
38. Macdonald JM, Grillo M, Schmidlin O, Tajiri DT, James TL. NMR spectroscopy and MRI investigation of a potential bioartificial liver. NMR Biomed 1998;11:55–66. [PubMed: 9608589]
39. Maharjan RP, Ferenci T. Global metabolite analysis: the influence of extraction methodology on metabolome profiles of *Escherichia coli*. Anal Biochem 2003;313:145–154. [PubMed: 12576070]
40. Tyagi RK, Azrad A, Degani H, Salomon Y. Simultaneous extraction of cellular lipids and water-soluble metabolites: evaluation by NMR spectroscopy. Magn Reson Med 1996;35:194–200. [PubMed: 8622583]
41. Chandrasekaran P, Seagle C, Rice L, Macdonald JM, Gerber DA. Functional analysis of encapsulated hepatic progenitor cells. Tissue Eng 2006;12:2001–2008. [PubMed: 16889528]
42. Gamcsik MP, Forder JR, Millis KK, McGovern KA. A versatile oxygenator and perfusion system for magnetic resonance studies. Biotechnol Bioeng 1996;49:348–354. [PubMed: 18623587]
43. Swanson MG, Keshari KR, Tabatabai ZL, Simko JP, Shinohara K, Carroll PR, Zektzer AS, Kurhanewicz J. Quantification of choline- and ethanolamine-containing metabolites in human

prostate tissues using (1)H HR-MAS total correlation spectroscopy. Magn Reson Med 2008;60:33–40. [PubMed: 18581409]

44. Karlsson J, Hulten B, Sjodin B. Substrate activation and product inhibition of LDH activity in human skeletal muscle. Acta Physiol Scand 1974;92:21–26. [PubMed: 4370414]
45. Kohler SJ, Yen Y, Wolber J, Chen AP, Albers MJ, Bok R, Zhang V, Tropp J, Nelson SJ, Vigneron DB, Kurhanewicz J, Hurd RE. In vivo 13 carbon metabolic imaging at 3T with hyperpolarized ^{13}C-1-pyruvate. Magn Reson Med 2007;58:65–69. [PubMed: 17659629]
46. Nicholas PC, Kim D, Crews FT, Macdonald JM. ^{1}H NMR-based metabolomic analysis of liver, serum, and brain following ethanol administration in rats. Chem Res Toxicol 2008;21:408–420. [PubMed: 18095657]
47. Gamcsik MP, Dubay GR, Cox BR. Increased rate of glutathione synthesis from cystine in drug-resistant MCF-7 cells. Biochem Pharmacol 2002;63:843–851. [PubMed: 11911835]
48. Balendiran GK, Dabur R, Fraser D. The role of glutathione in cancer. Cell Biochem Funct 2004;22:343–352. [PubMed: 15386533]
49. Macdonald JM, Kurhanewicz J, Dahiya R, Espanol MT, Chang LH, Goldberg B, James TL, Narayan P. Effect of glucose and confluency on phosphorus metabolites of perfused human prostatic adenocarcinoma cells as determined by ^{31}P MRS. Magn Reson Med 1993;29:244–248. [PubMed: 8429789]
50. Masson S, Quistorff B. The ^{31}P NMR visibility of ATP in perfused rat liver remains about 90%, unaffected by changes of metabolic state. Biochemistry 1992;31:7488–7493. [PubMed: 1510935]
51. Narayan KS, Moress EA, Chatham JC, Barker PB. ^{31}P NMR of mammalian cells encapsulated in alginate gels utilizing a new phosphate-free perfusion medium. NMR Biomed 1990;3:23–26. [PubMed: 2390450]
52. Gross JD, Constantinidis I, Sambanis A. Modeling of encapsulated cell systems. J Theor Biol 2007;244:500–510. [PubMed: 17049564]

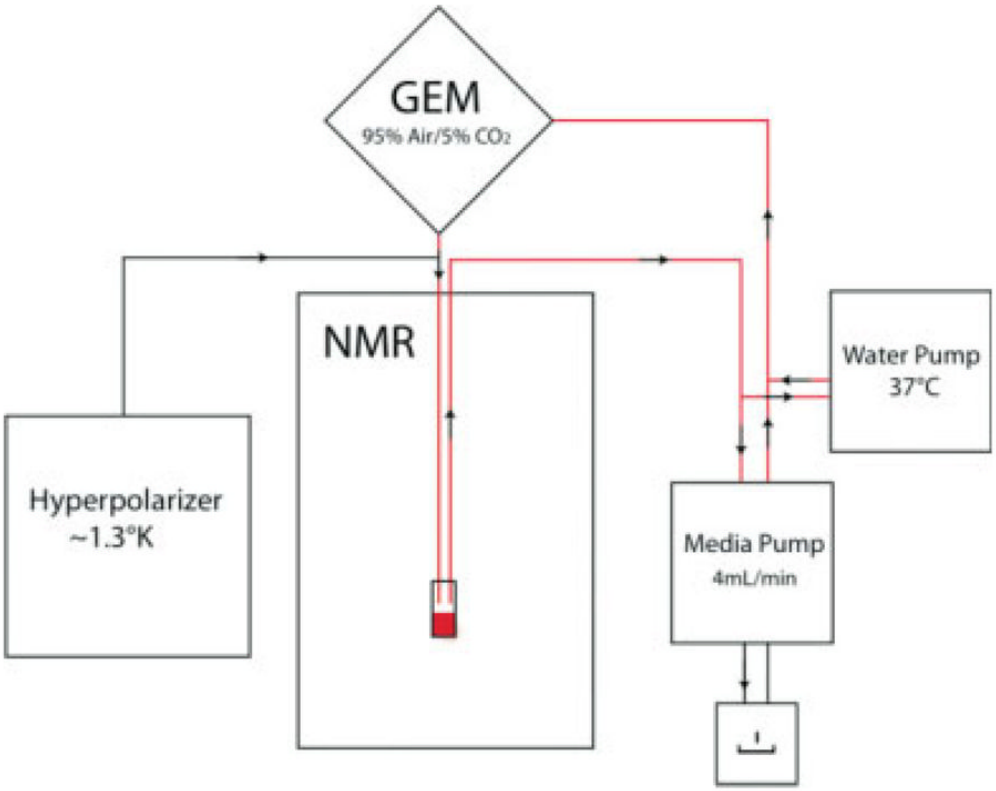

FIG. 1.
Schematic of bioreactor setup. The red line indicates the flow of media as it recirculates in the bioreactor. GEM, gas exchange module.

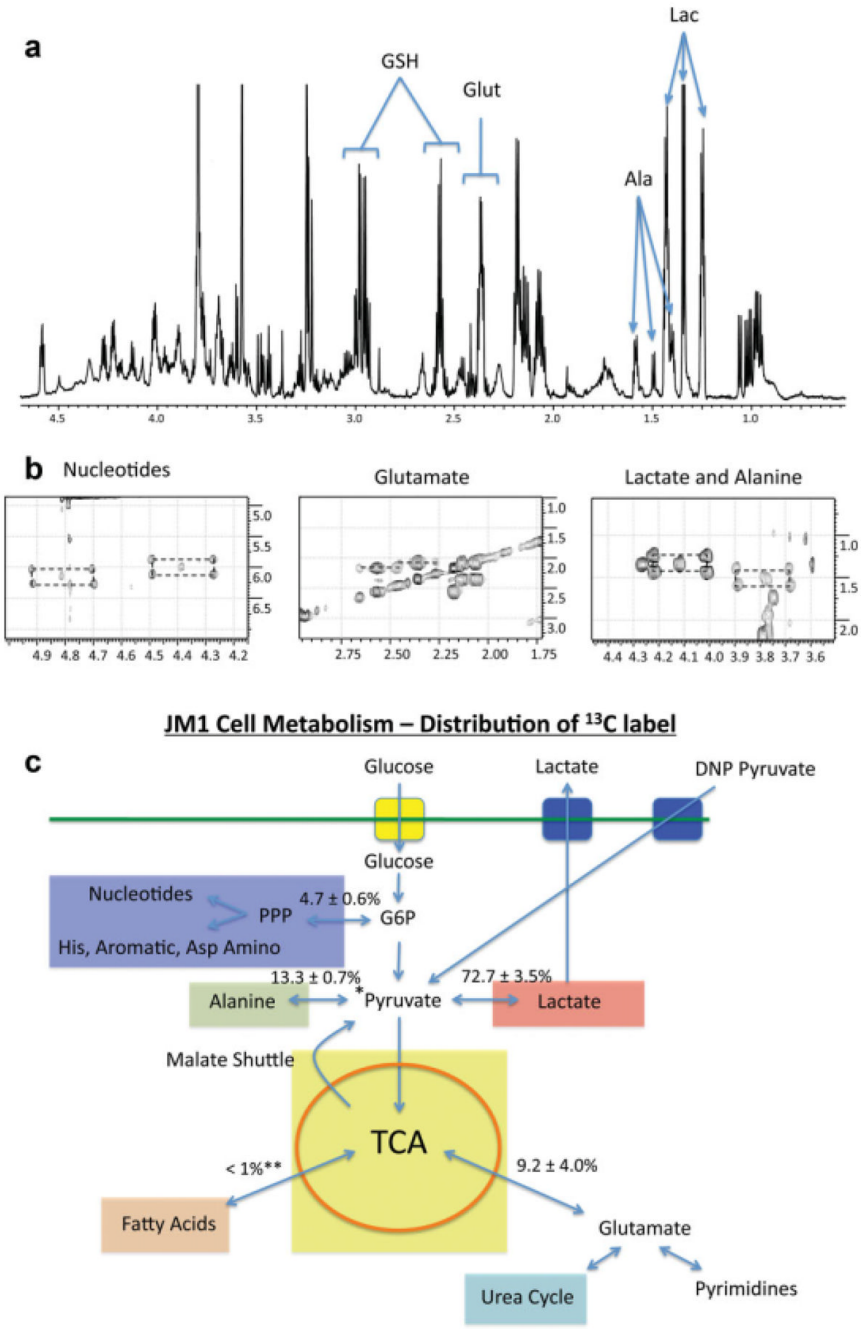

FIG. 2.

a: Representative ^{1}H spectrum of water soluble metabolites at 23 h. **b:** Representative total correlation spectroscopy spectra showing FE of compounds by infusion of uniformly labeled ^{13}C-glucose. **c:** Cancer metabolic phenotype. Percentages ± standard of deviation are shown for the distribution of ^{13}C compounds in the cell as a result of medium supplemented with uniformly labeled ^{13}C glucose. The DNP pyruvate arrow denotes the mechanism for infusion of hyperpolarized pyruvate and its relationship to the distributions measured in 2D cultures of JM1 cells. Yellow box: glucose transporter (GLUT) (1,3,4); blue box: MCT: monocarboxylate transporter (predominantly 4). Light blue: pentose phosphate pathway (PPP) flux into ribose etc. Pink box: anaerobic/aerobic glycolysis. Light yellow box: tricarboxylic

acid cycle (TCA). Aqua box: urea cycle. Light red box: fatty acid synthesis as a result of exchange with TCA pathway. Light green box: flux through ALT and into protein synthesis. *Indication of methodology of hyperpolarized pyruvate. **In lipid extracts, carbon labeling was below detection.

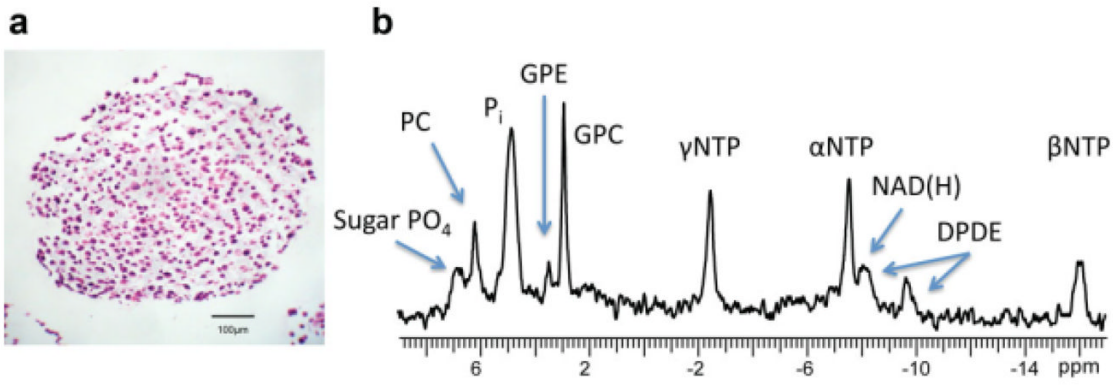

FIG. 3.

Representative ^{31}P and histology of encapsulated beads. **a:** Hematoxylin and eosin–stained section of a 500-μm bead of encapsulated JM1 cells at 20× magnification. **b:** representative ^{31}P spectrum at 4 h postencapsulation and perfusion in the bioreactor. γNTP, αNTP, and βNTP represent the phosphates of the NTPs. PC, phosphocholine; Pi, inorganic phosphate (this peak is composed of the P_i inside and outside the cell); GPC, glycerolphosphocholine; GPE, glycerophosphoethanolamine; NAD(H), nicotinamide (reduced and oxidized); DPDE, diphosphodiesters, most commonly UDP glucose; sugar PO_4, sugar phosphate groups.

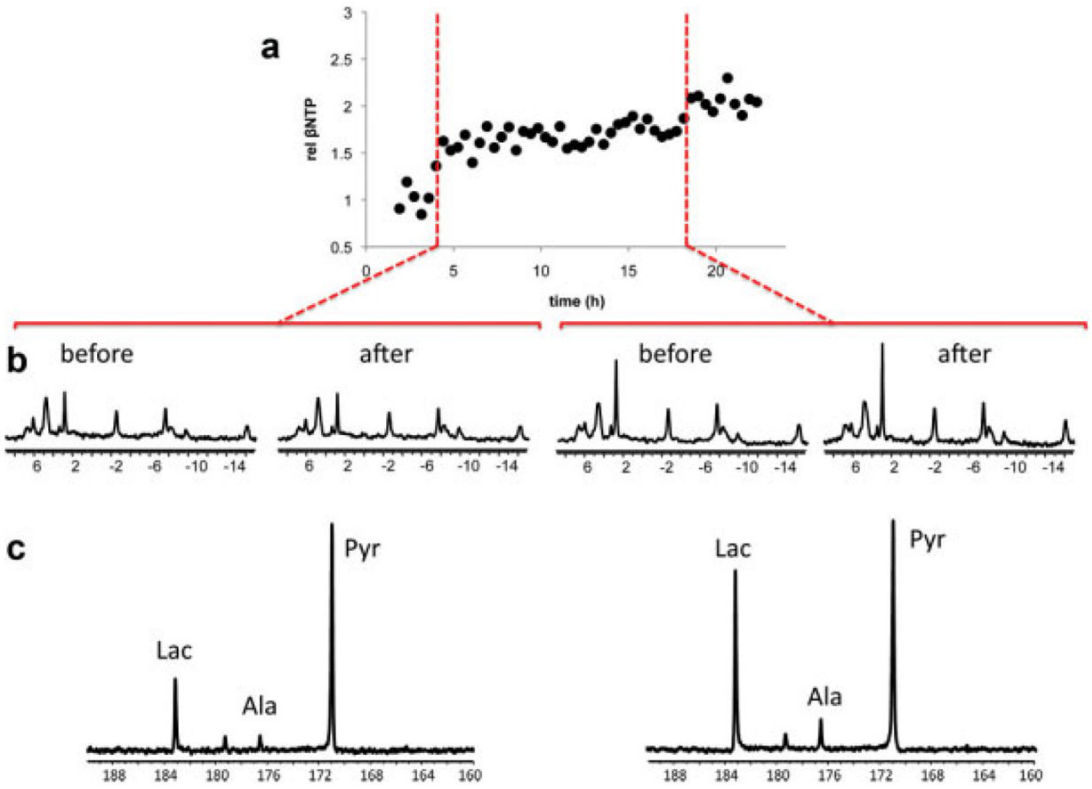

FIG. 4.

^{31}P monitoring and dynamic ^{13}C spectra of JM1 cells. **a:** A ^{31}P time course showing the relative changes in βNTP as JM1 cells encapsulated at a concentration of 127 × 10^6 cells/mL change over time. **b:** Before and after ^{31}P spectra at the dictated time points of injection of 1 mL of 7.1-mM hyperpolarized pyruvate, 4 h and 18.5 h, respectively. **c:** ^{13}C spectra at 90 sec postinjection, demonstrating the conversion of pyruvate (171 ppm) to lactate (182 ppm) and alanine (175 ppm).

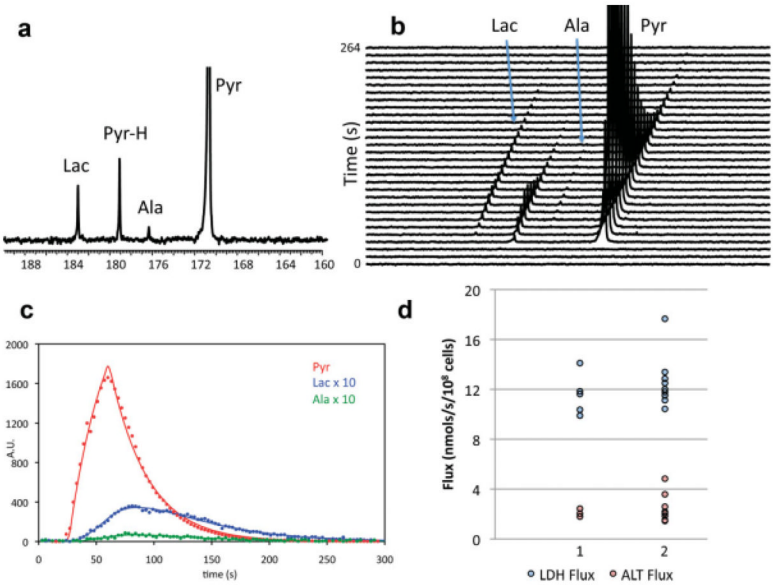

FIG. 5.

Study in bioreactor of JM1 cells at a concentration of 50×10^6 cells/mL. **a:** ^{13}C spectrum acquired at 84 sec postinjection of 2 mL of 3.56-mM hyperpolarized pyruvate. **b:** Every third ^{13}C spectrum acquired demonstrating the hyperpolarized ^{13}C labeling of lactate (Lac) and alanine (Ala) as result of ^{13}C pyruvate (Pyr). Pyruvate hydrate (Pyr-H) is also shown, which is in equilibrium with pyruvate. **c:** Red dots, pyruvate; blue dots, lactate ×10; green dots, alanine ×10; the lines for each respective color are the fits as a result of the flux model for ^{13}C labeling of lactate and alanine via LDH and ALT, respectively. **d:** LDH (blue) and ALT (red) flux measurements for days 1 and 2 in the bioreactors.

Table 1

Glucose, Pyruvate, Glutamate, Glutamine, Alanine, Lactate, X-Purine, X-Pyrimidine, and Glutathione Concentrations in the Cell Methanol Extract (t = 23 h), Medium From 2D Cultures at 23 h, and From the Initial Medium Formulation

	Initial medium (μmols/15 mL)	2D cultures (methanol) (μmols/10^6 cells)	2D cultures (media) (μmol)
Glucose	249	—	111.84 ± 7.61
Pyruvate	15	—	—
Glutamate	0	0.037 ± 0.002	—
Glutamine	60	—	53.95 ± 0.63
Glutathione	0	0.046 ± 0.004	—
Alanine	0	0.026 ± 0.003	17.07 ± 1.53
Lactate	0	0.091 ± 0.007	242.57 ± 15.79
X-Purine	0	0.002 ± 0.0004	—
X-Pyrimidine	0	0.002 ± 0.0005	—

— Indicates compounds that were not detected by NMR.